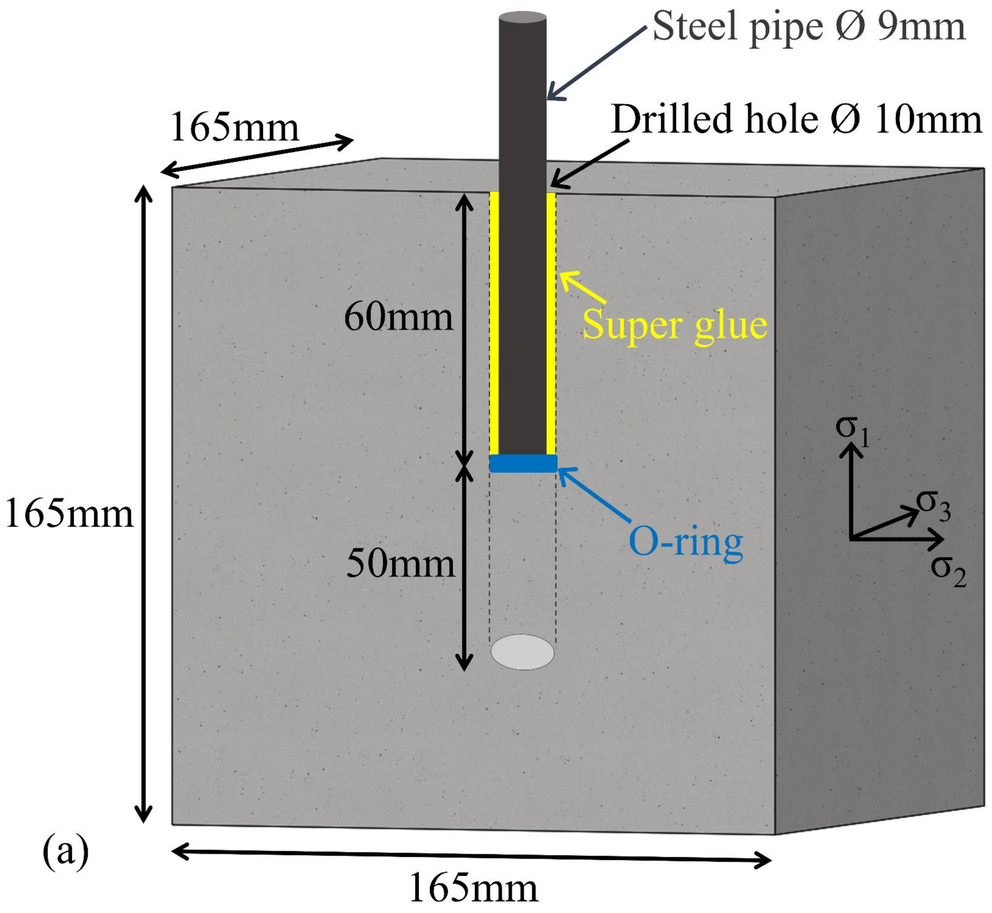

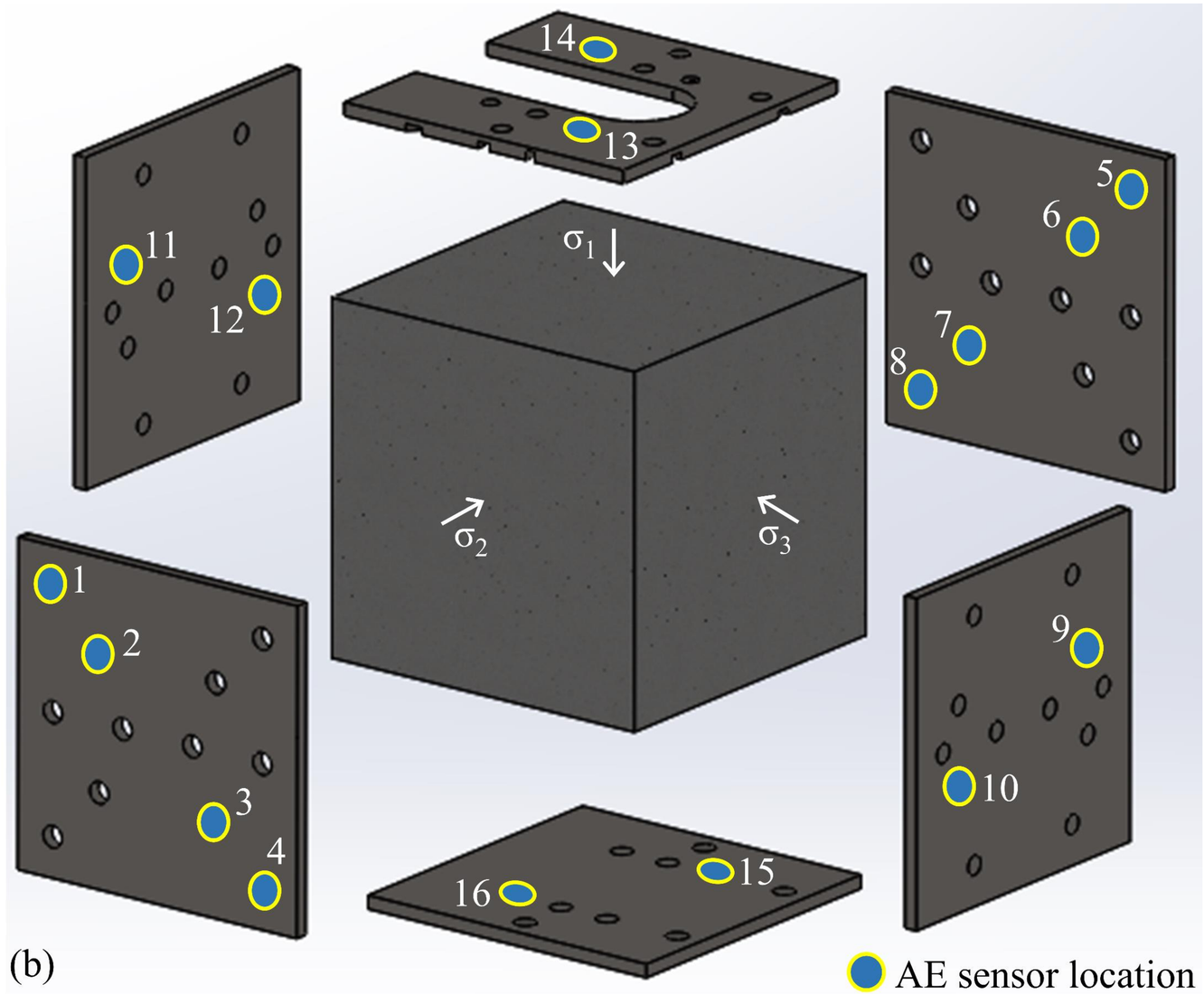

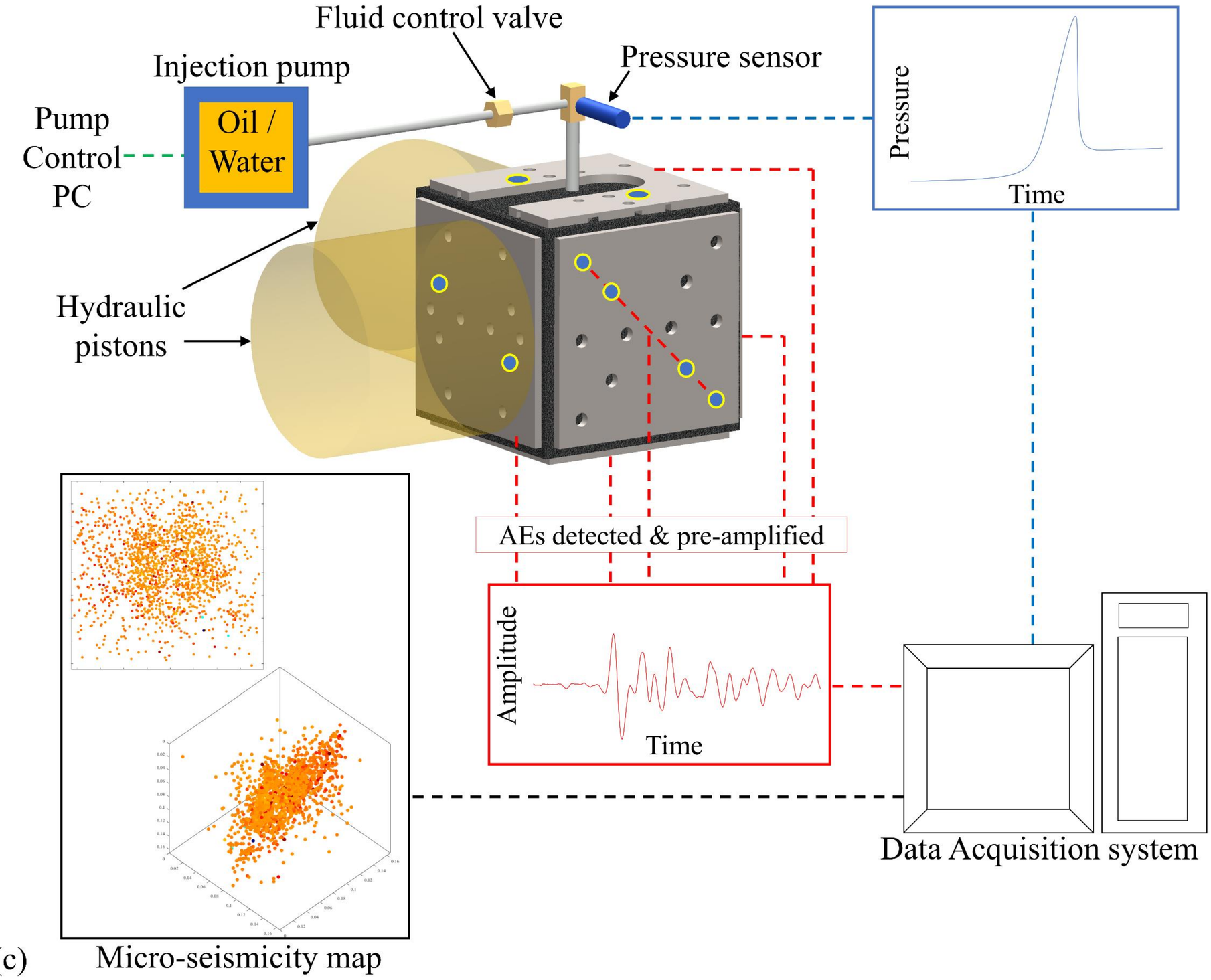

Figure 1. (a) Schematic of the specimen and borehole configuration used for the HF experiments. A small borehole with a radius of 5 mm was selected with respect to its distance to the boundaries of the cubic block (82.55 mm) (b) The location of 16 Nano-30 AE sensors, with an aperture of 8 mm, selected for the HF experiments providing sufficient coverage of the entire block. Eight sensors were located in the direction of fracture propagation (σ2), and four each in the σ3 and σ1 directions (c) Schematic of the complete experimental setup. The data from the AE sensors were amplified and recorded in the computer for post-experiment analysis. The data from the hydraulic pistons and the pressure sensor, located near the borehole entrance, was also recorded in the same computer to achieve synchronization between the pressure, confining stress, and the AE data

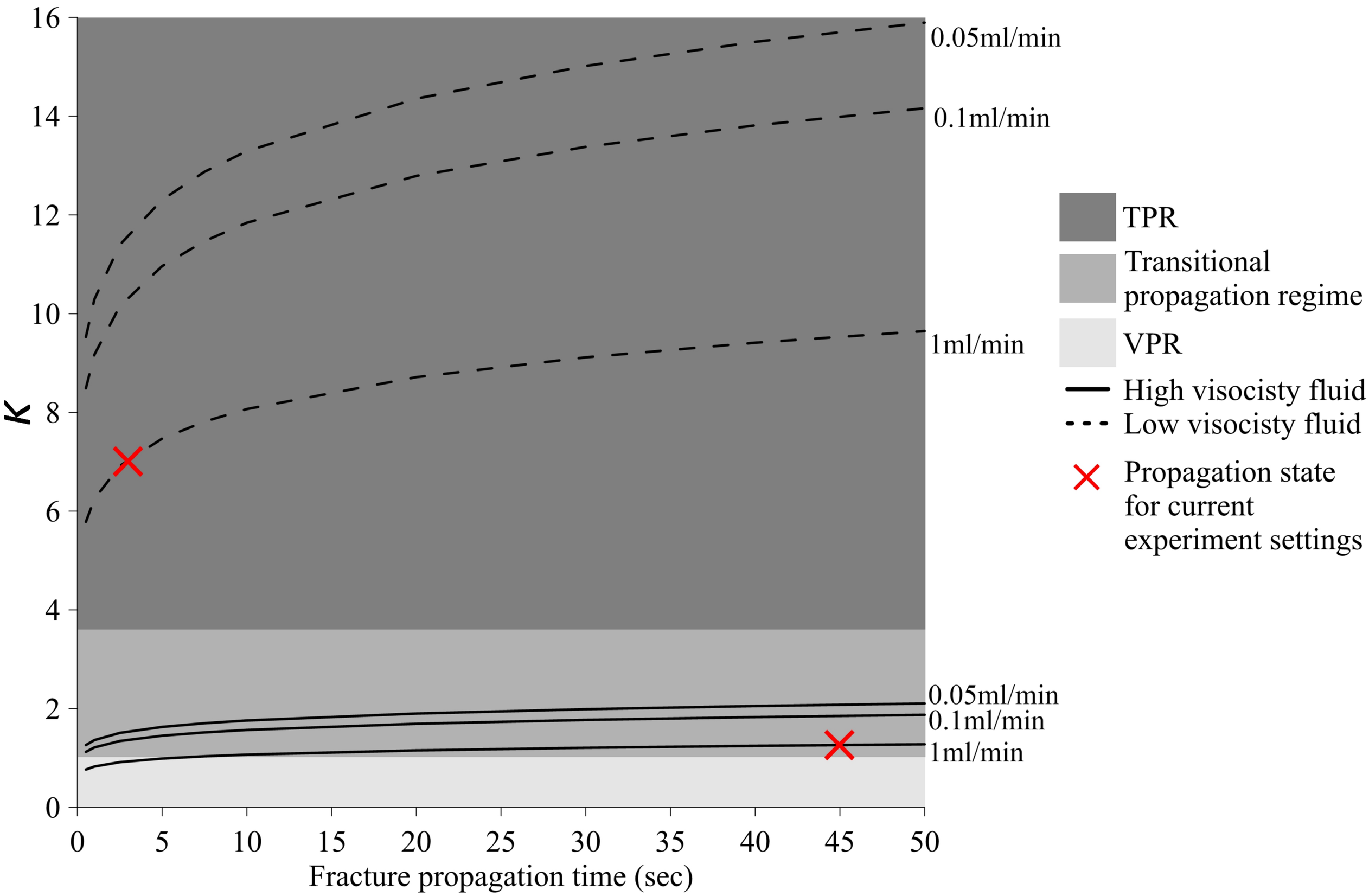

Figure 2. The dimensionless toughness parameter, ***κ***, determined for different experimental settings and fracture propagation times and different injection rates. High viscosity injections are presented in solid lines and low viscosity injections in dashed lines. The points in the graph (X) indicates the determined state of the HF operation for experimental settings used in this study. A ***κ*** value of 1.27 corresponded to an almost viscosity dominated propagation regime, whereas a value of 7.0 resulted in the toughness dominated propagation regime

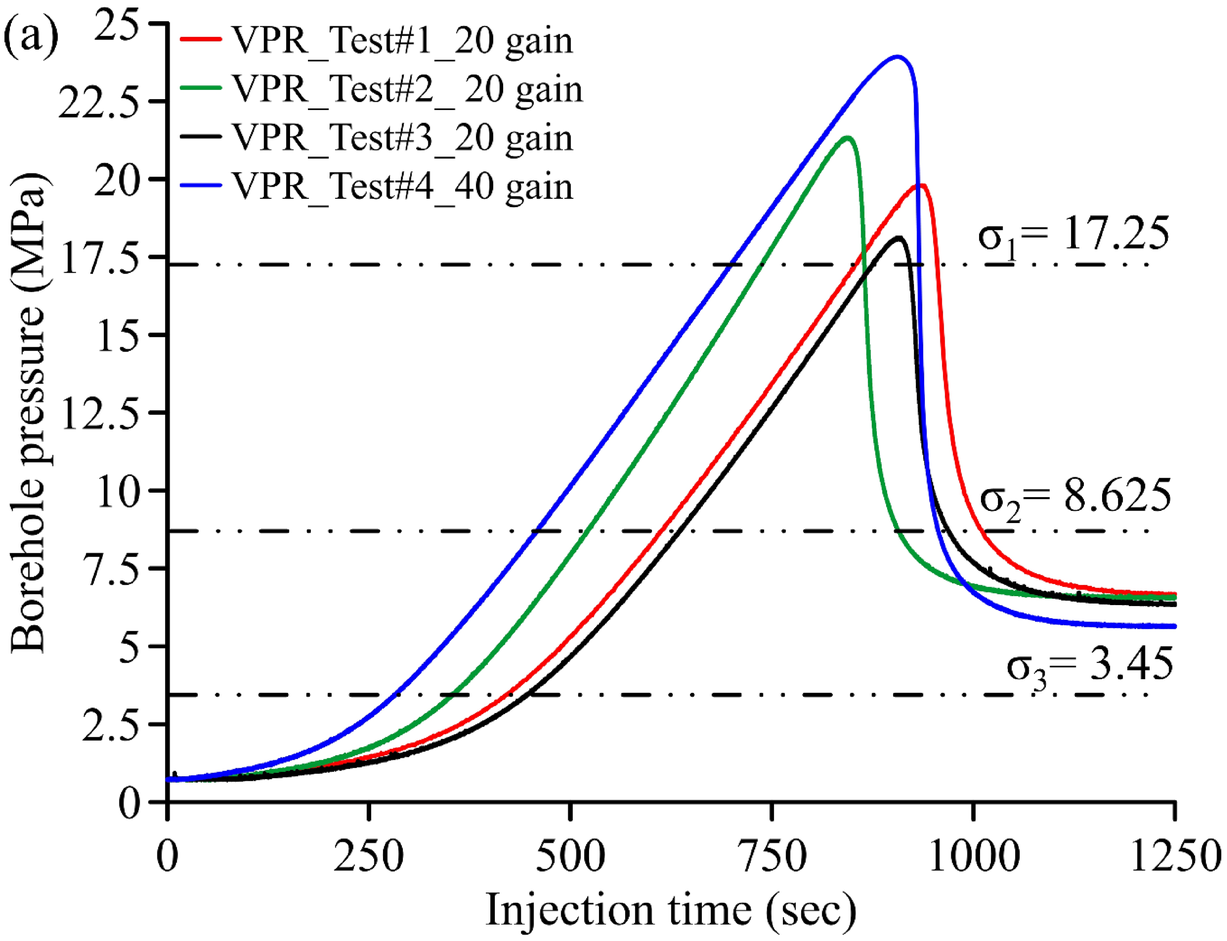

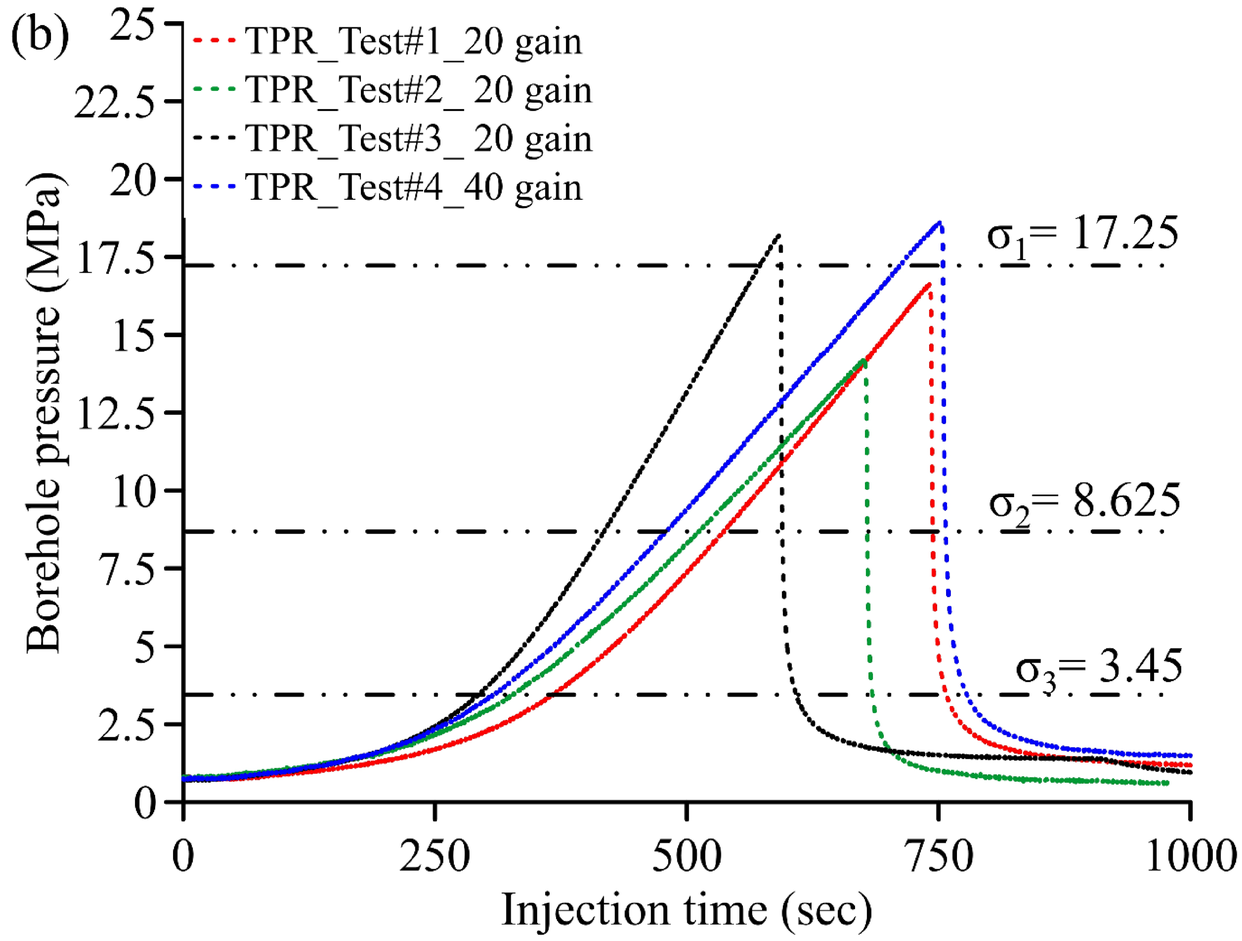

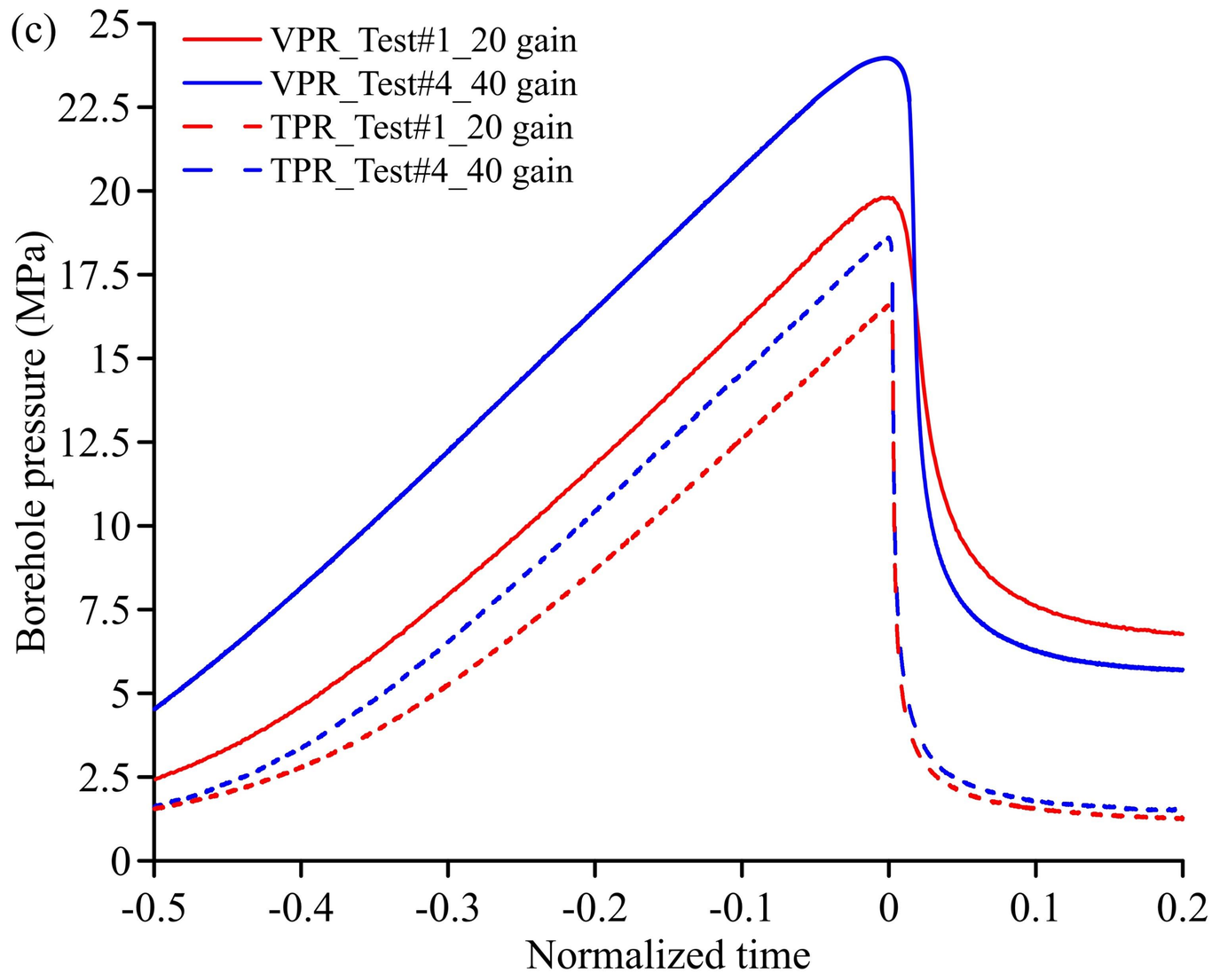

Figure 3. Borehole pressure evolution with actual experimental time for different (a) VPR and (b) TPR experiments. (c) Borehole pressure evolution against normalized time for a pair of VPR and TPR experiments. On average, VPR experiments resulted in higher BPs and gradual pressure drop after the breakdown, relative to TPR experiments. For all the experiments, the borehole pressure reached a constant value after breakdown. However, this pressure was higher for VPR experiments (~6.5 MPa) as compared to the TPR experiments (~1), which represents the ease with which the injection fluid can excrete out from the generated fracture

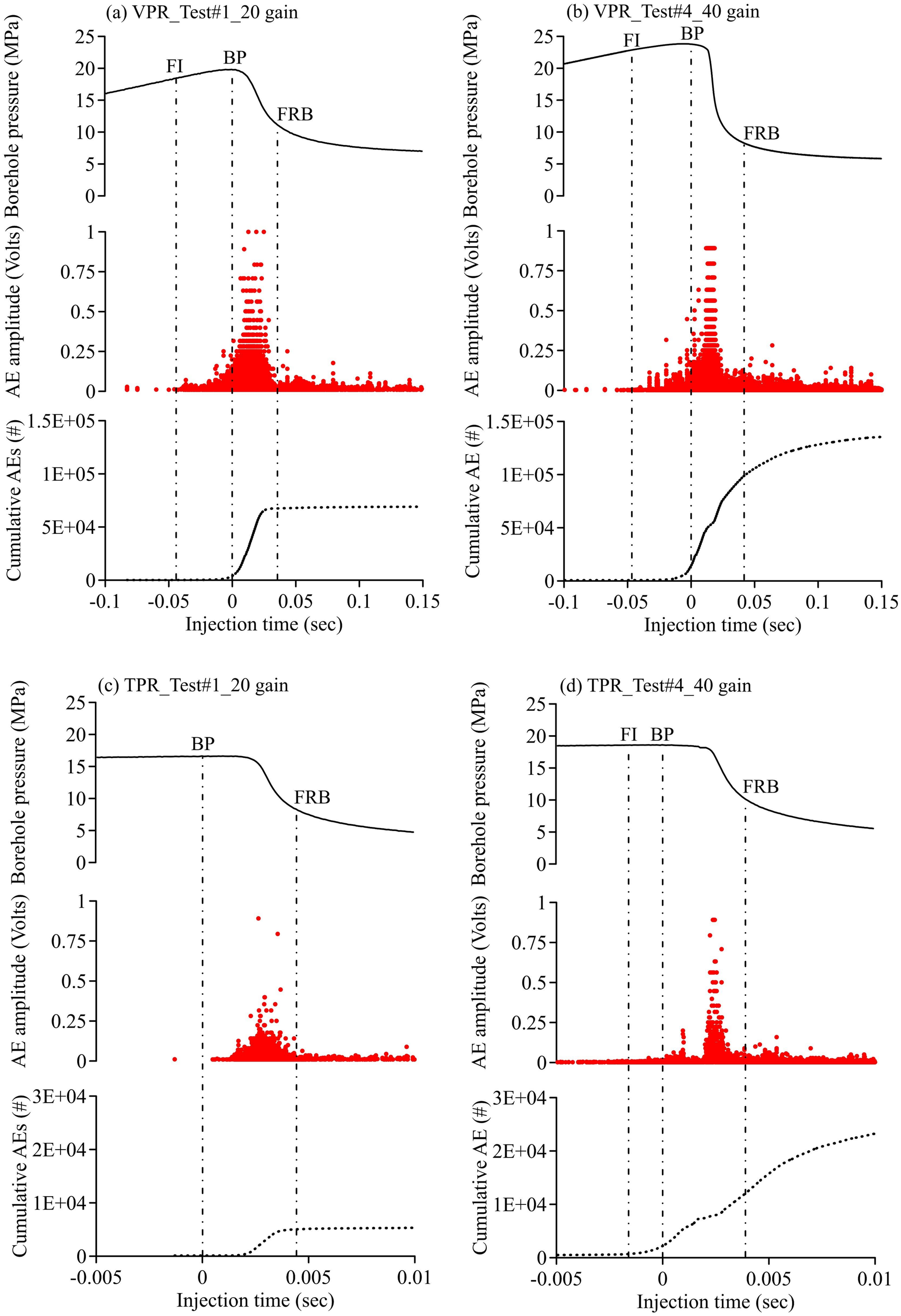

Figure 4. Detected AEs and the cumulative AEs along with the borehole pressure evolution against normalized time for (a) VPR_Test#1_20 gain, (b) VPR_Test#4_40 gain, (c) TPR_Test#1_20 gain and (d) TPR_Test#4_40 gain; FI (fracture initiation) represents the point where the AE rate started to increase, BP (breakdown pressure) was the highest recorded borehole pressure for a particular experiment, and FRB (fracture reaching boundaries of the specimen) was determined using the pressurization rate ($\partial P/\partial t$), detected AEs and the $\sigma 3$ stress measurements (see figure 5). AEs amplitude from the 40-gain experiment was divided by 10 for comparison with the 20-gain experiment. The number of AEs detected for VPR and TPR experiments, with 40-gain setting, were approximately 2 and 7 times higher than those detected with the 20-gain VPR and TPR experiments, respectively

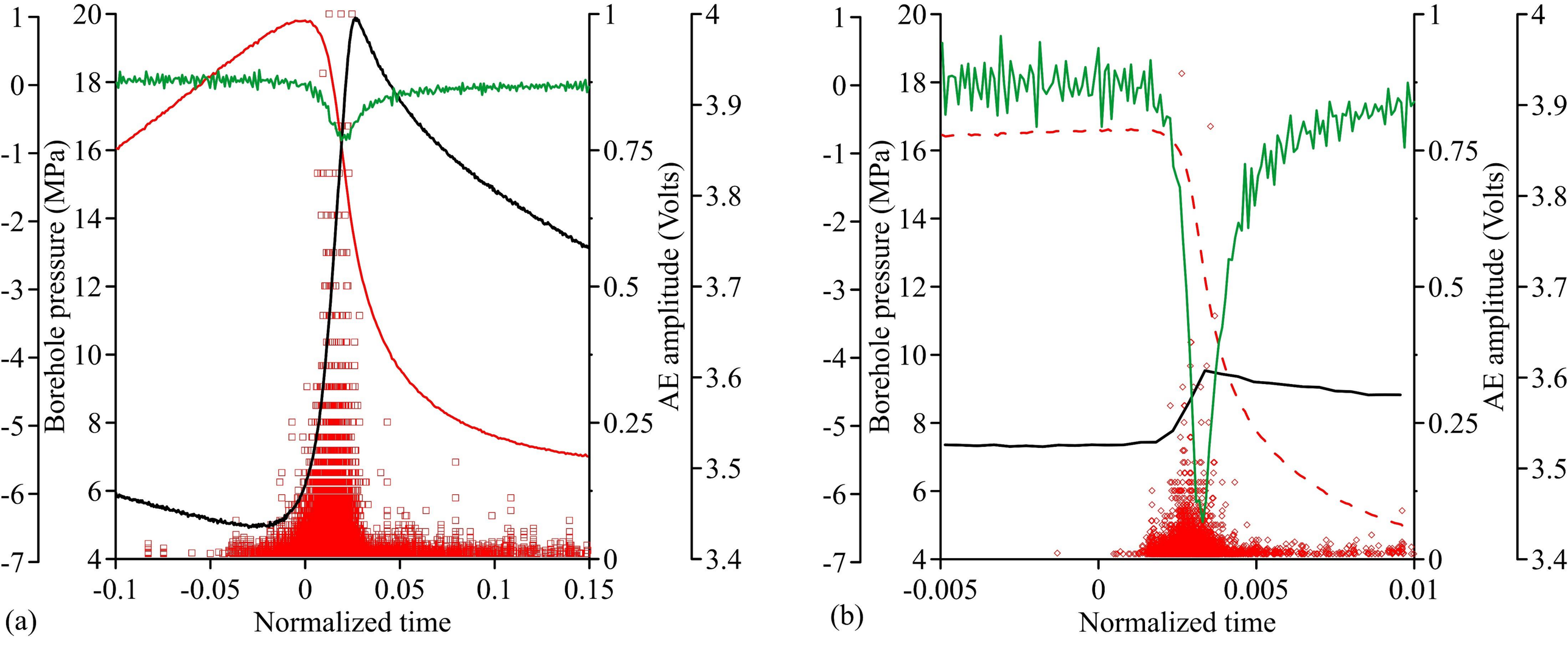

Figure 5. Progression of ∂P/∂t and σ3 stress with detected AEs for (a) VPR_Test # 1_20 gain and (b) TPR_Test # 1_20 gain. The peak increase in σ3 almost coincided with the termination of significant AE activity for all the experiments. Also, this reduction of AE rate to a minimum overlapped with the inflection point in ∂P/∂t as it approached a constant value

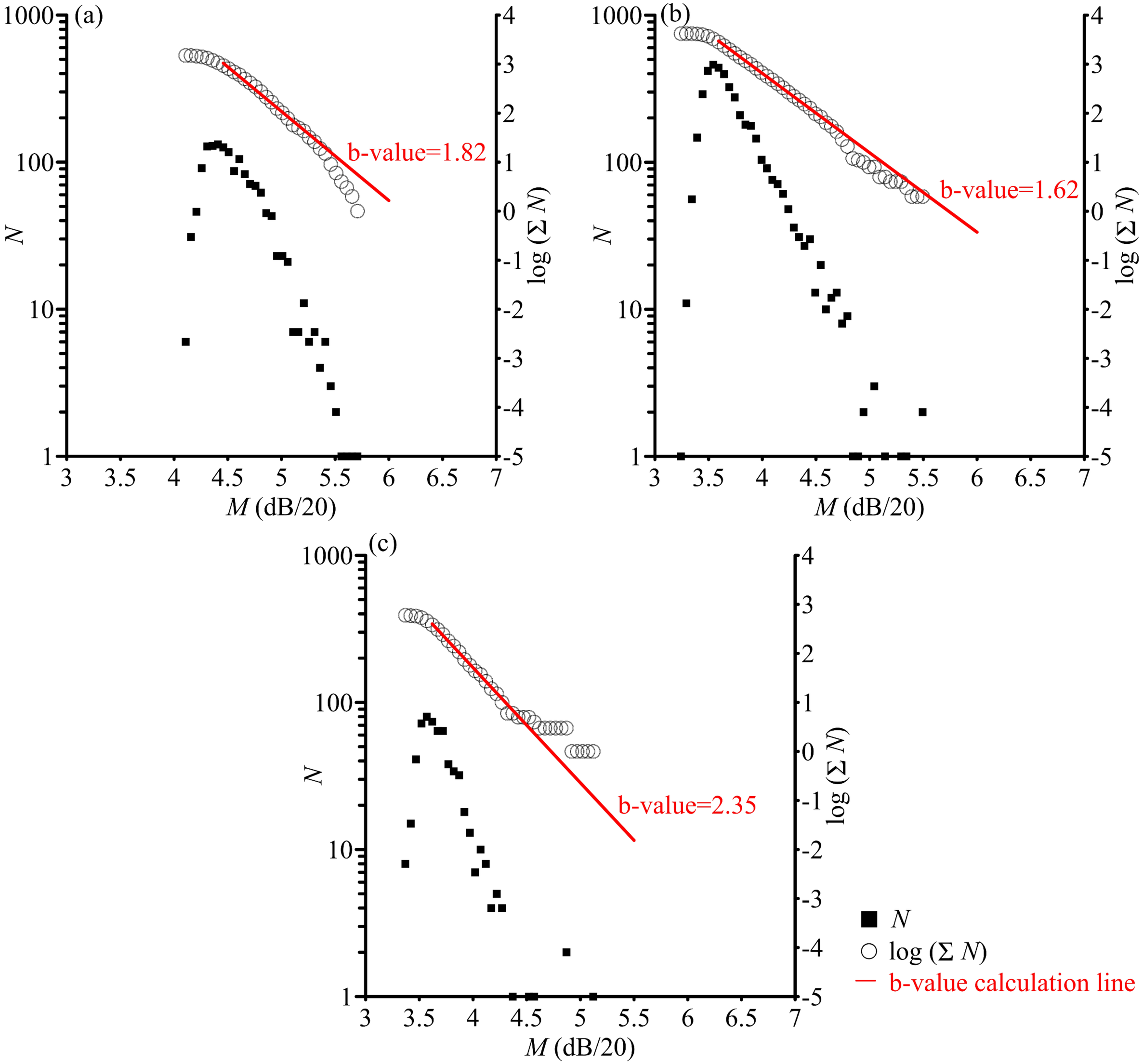

Figure 6. b-value calculation for (a) VPR_Test#1_20 gain, (b) VPR_Test#4_40 gain, and (c) TPR_Test#4_40 gain experiments. N is the number of seismic events equal to or greater than a given magnitude (M). M was obtained by dividing the determined focal amplitude in dB by 20 and $\Delta Mbin$ was selected as 0.05. The b-value was determined for the linear portion of the log (Σ N) and the M plot

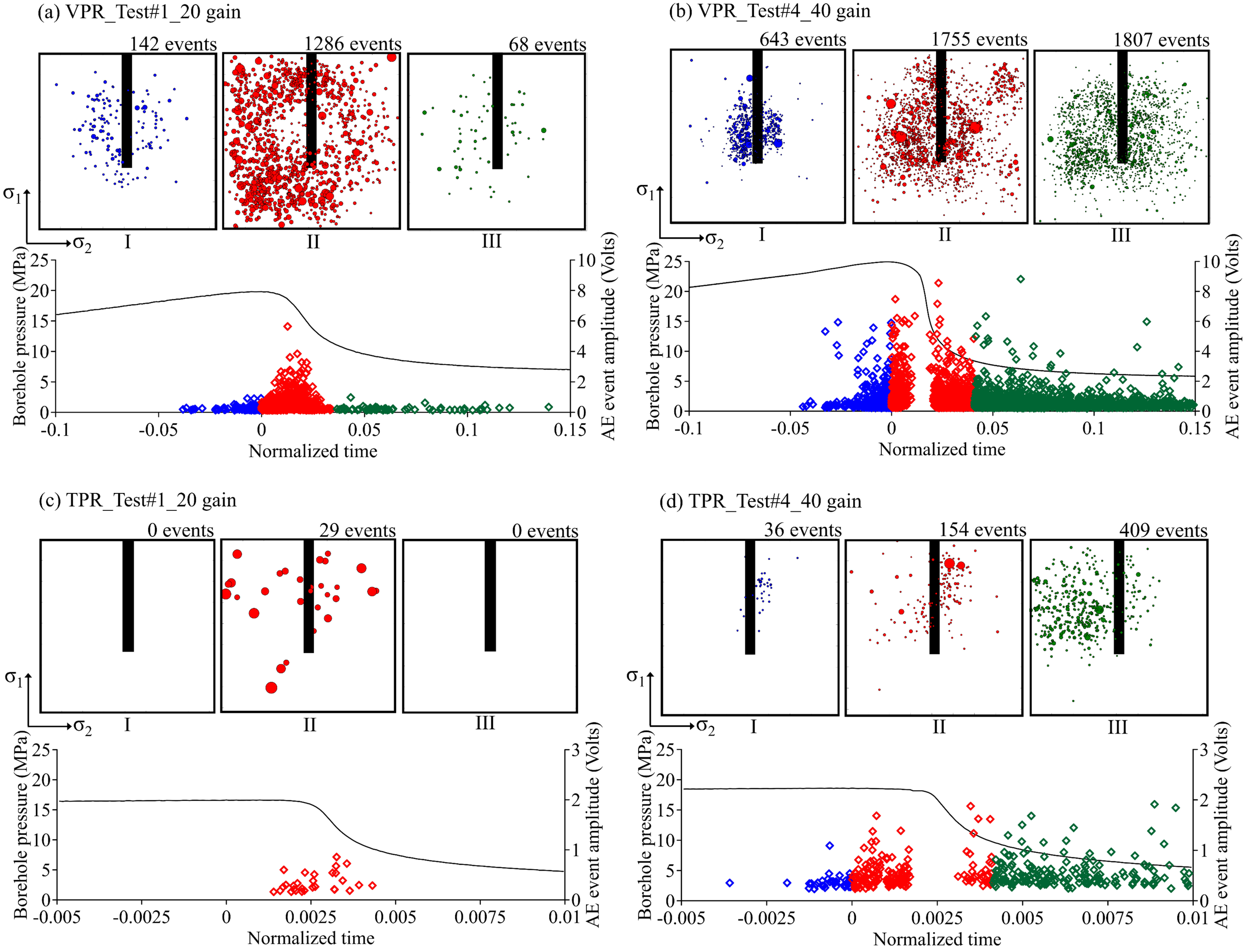

Figure 7. Spatiotemporal evolution of the AE events at different stages of the HF for (a) VPR_Test#1_20 gain, (b) VPR_Test#4_40 gain, (c) TPR_Test#1_20 gain, and (d) TPR_Test#4_40 gain; Phase (I) initiation to breakdown, (II) breakdown to fracture reaching boundaries of the specimen, and (III) the post fracturing phase. The size of the circles represents the relative AE event amplitude in any particular experiment. The 40-gain experiments were better at capturing the phase I and the post fracturing phase III periods. AE events were only detected during phase II for the TPR_Test#1_20_gain experiment

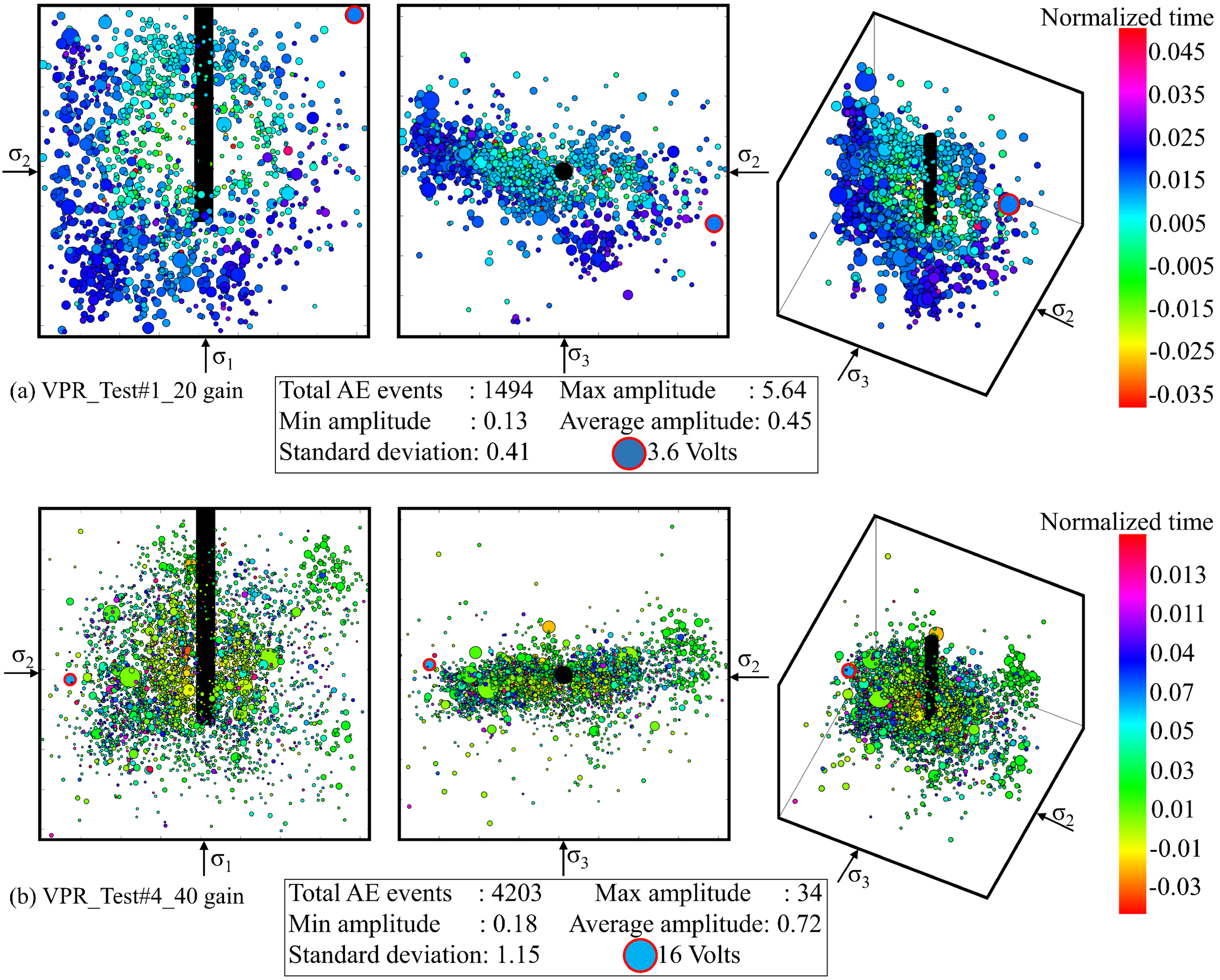

(a) VPR_Test#1_20 gain

(b) VPR_Test#4_40 gain

Figure 8. 2D and 3D view of the complete HF propagation for the (a) VPR_Test#1_20 gain, (b) VPR_Test#4_40 gain. The HF propagated almost perpendicular to the minimum stress (σ3) for both experiments. The occurrence of the AE events with respect to the normalized time is indicated through the colorbar. Majority of the detected AE events were in the blue and green shade in (a) and (b), respectively, which indicates that 40-gain setting was able to comprehensively capture the initial HF portion, whereas the 20-gain was better at identifying the later portion of the HF propagation

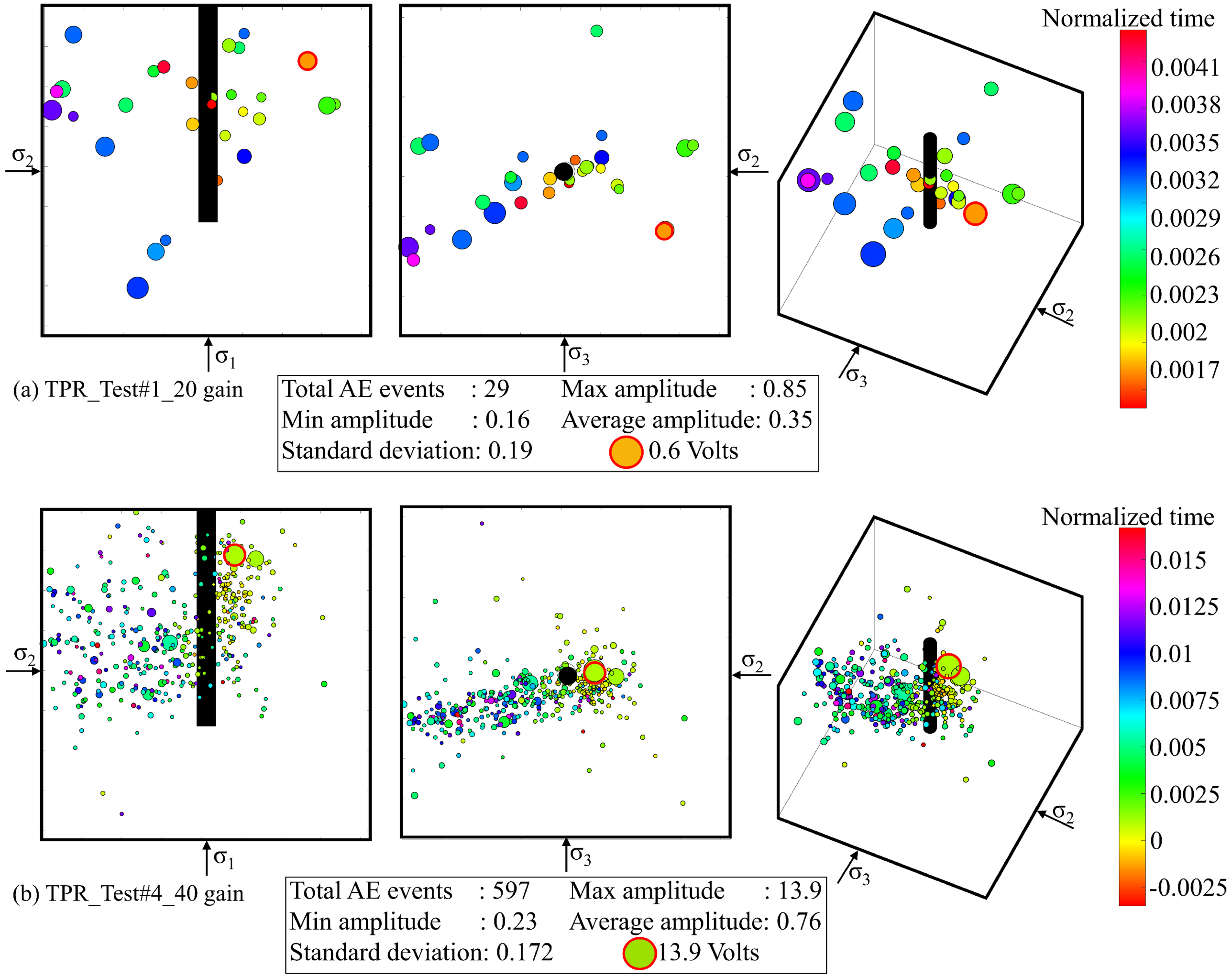

(a) TPR_Test#1_20 gain

(b) TPR_Test#4_40 gain

Figure 9. 2D and 3D view of the complete HF propagation for (a) TPR_Test#1_20 gain and (b) TPR_Test#4_40 gain. The occurrence of the AE events with respect to the normalized time is indicated through the colorbar. In comparison to the VPR experiments, the detected AE events in the TPR experiments were widely dispersed over the normalized time color spectrum

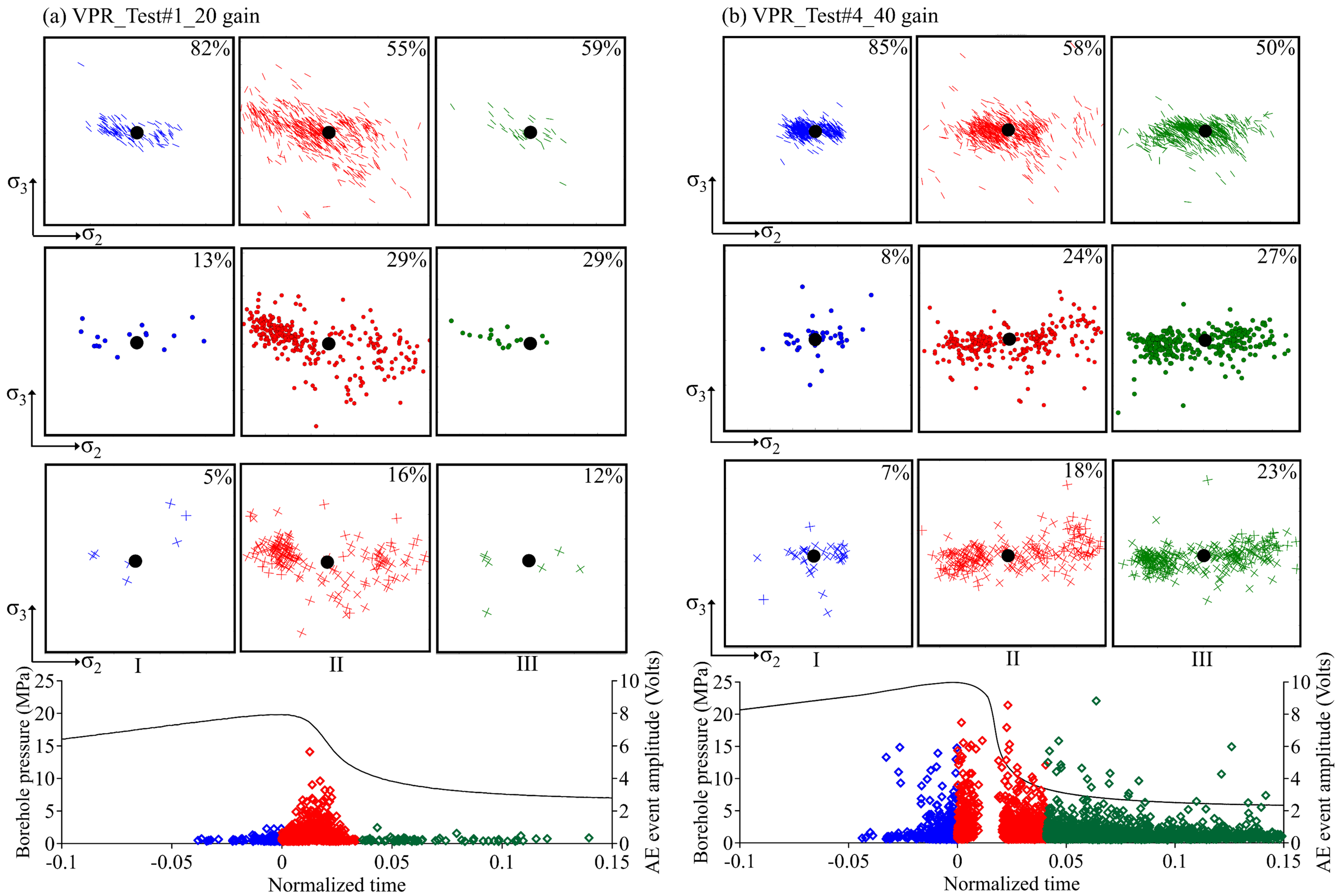

Figure 10. Damage mechanisms determined for different phases for VPR_Test#1_20 gain and (b) VPR_Test#4_40_gain experiments; tensile, mixed and shear mode in the top, middle and bottom rows respectively. The percentage of tensile events in the initiation to breakdown phase was relatively high. However, this percentage decreased as the fracture propagated away from the borehole

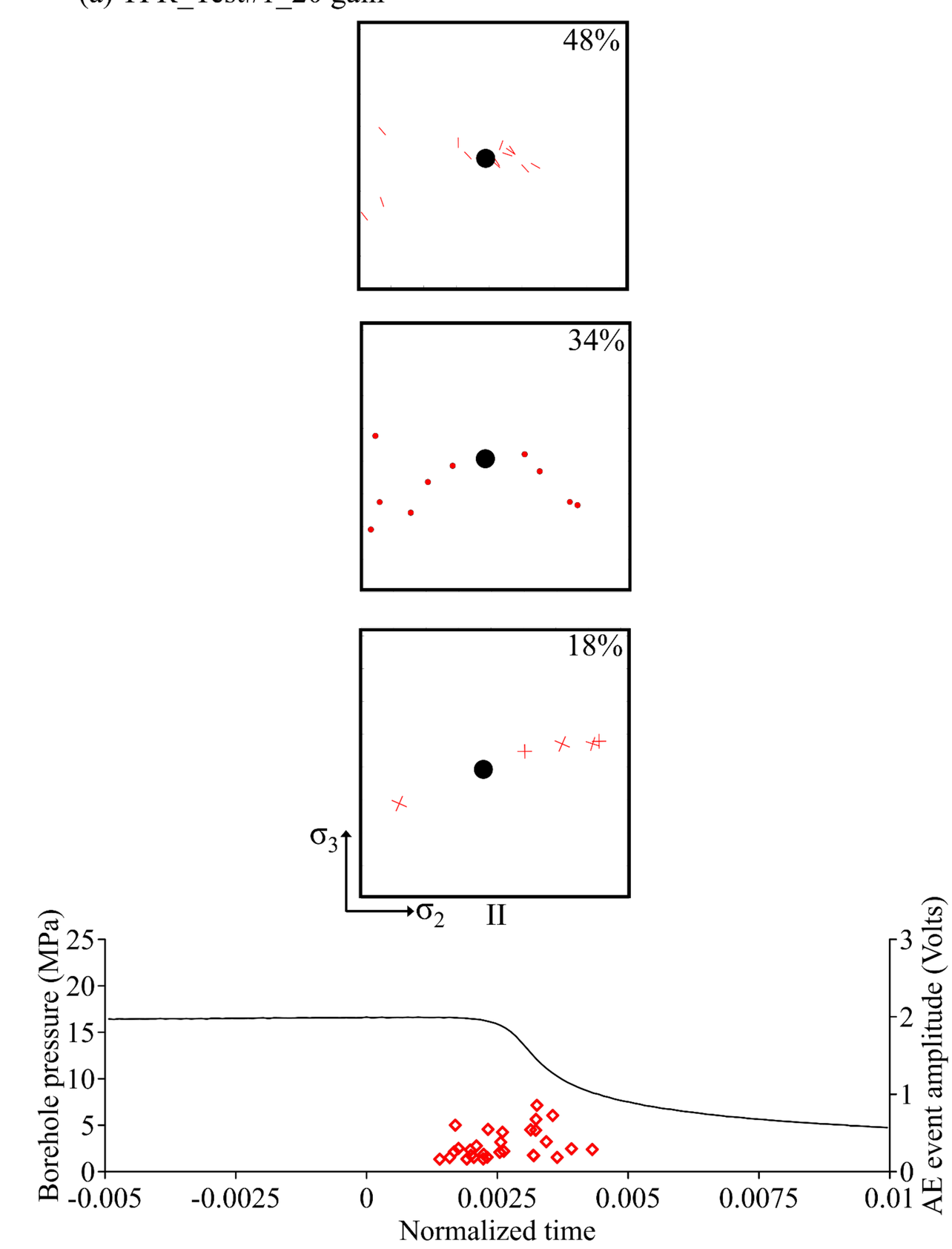

Figure 11. Damage mechanisms determined for different phases for (a) VPR_Test#1_20_gain and (b) VPR_Test#4_40_gain experiments; tensile, mixed and shear mode in the top, middle and bottom rows respectively. AE events were only detected in phase II of the 20-gain experiment (a), where tensile dominance near the borehole region could be observed. The absence of AE events pointed towards the saturation of the AE system and the relatively high percentage of tensile events in phase II of the 40-gain experiment (b).

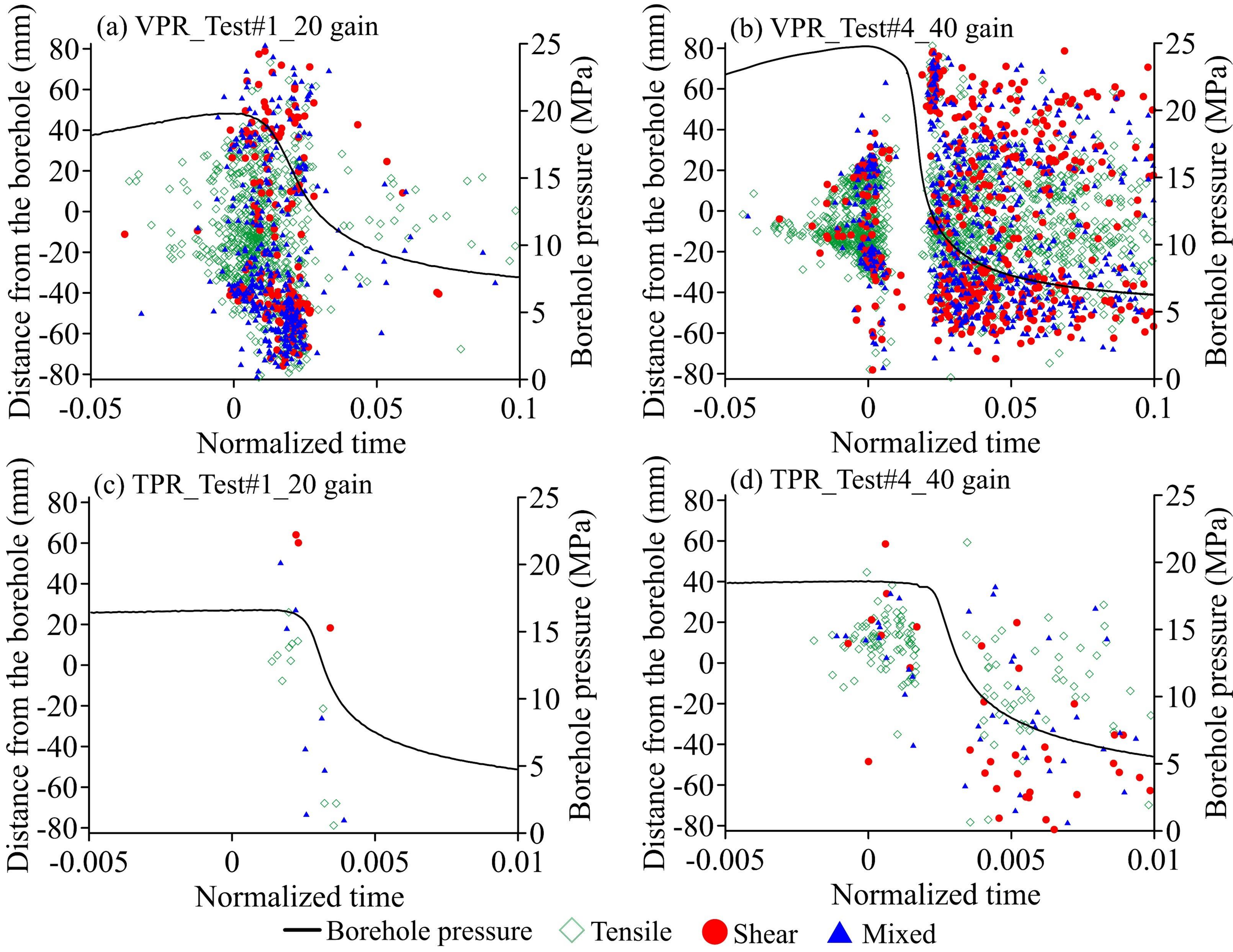

Figure 12. Damage mechanisms (tensile, shear, and mixed mode) with distance from the borehole for (a) VPR_Test#1_20 gain (b) VPR_Test#4_40 gain (c) TPR_Test#1_20 gain and (d) TPR_Test#4_40 gain. The distance is from the center (0) to the boundaries of the specimen in the direction of fracture propagation. Relatively more events were detected in the post fracturing phase by the 40-gain experiments. The absence of events in (b) and (d) for a small period is due to the saturation of the AE system